arXiv:1607.04535v1 [cond-mat.mes-hall] 15 Jul 2016

Theory of spin-coherent transport through a defect spin state in a metal/ferromagnet tunnel junction during ferromagnetic resonance

N. J. Harmon* and M. E. Flatté†
Department of Physics and Astronomy and Optical Science and Technology Center, University of Iowa, Iowa City, Iowa 52242, USA
(Dated: July 18, 2016)

We describe the coherent interaction between a defect spin at the interface of a ferromagnet and a nonmagnetic material, under bias and when the magnetization of the ferromagnetic contact precesses during ferromagnetic resonance. The magnet filters charge carriers by preferentially allowing in parallel spins, which leads to a dynamic spin accumulation on the defect. Local effective fields acting on the defect spin site modify the defect spin's precession, which also modifies the charge current through the defect. This new form of current-detected spin resonance reveals the local environment of the defect, and thus can yield the defect identity.

Defects at nonmagnet/ferromagnet (NM/FM) interfaces drive defect-associated spin pumping [1–3], thermal spin transport [4], and small-field magnetoresistance under electrical bias [5–7]. Spin-coherent defects have been electrically detected in precisely-designed junctions such as a magnetic scanning tunneling microscope tip [8] or a phosphorus dopant manipulated with a dynamic magnetic field in a silicon transistor [9]. Considerable interest lies in the emerging field of "quantum spintronics" which seeks to engineer and manipulate single coherent spin systems for the sake of quantum-enhanced sensing/imaging technologies and quantum computing [10]. Identifying the origin of minute numbers of unintentional defects in an electrical device is challenging, as microscopies such as scanning tunneling microscopy often distort the environment of the defect due to space-charge effects, and many defects produce similar topographic or charge-density features. Conventional electron spin resonance (ESR) requires macroscopic volumes and thus cannot resolve fewer than $\sim 10^{10}$ spins [11]. Alternative schemes like electrically detected magnetic resonance (EDMR) have achieved single spin detection in a quantum dot [12] but using the technique for defect spin detection has not managed to resolve fewer than ~ 100 spins [13].

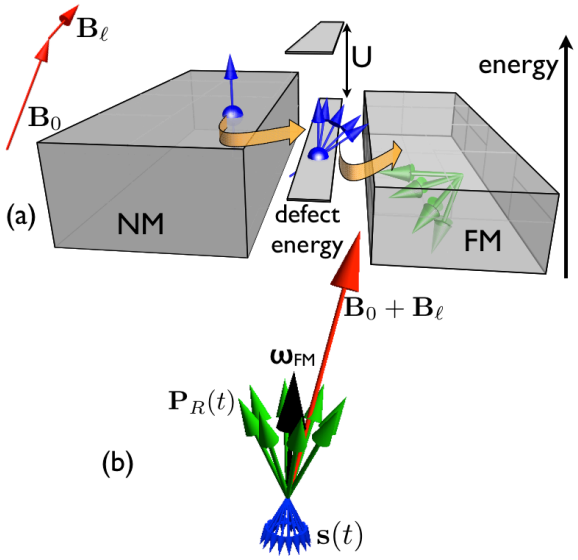

FIG. 1. (a) Diagram of the nonmagnetic metal (NM)/insulator (I)/ferromagnet (FM) junction for FM magnetization oscillating in time (denoted by green arrows). The spin (blue arrows) of the defect precesses in an applied and a local magnetic field, $\boldsymbol{\omega}_0 + \boldsymbol{\omega}_\ell$. (b) Schematic of vectors relevant for coherent defect detection.

Here we predict observable coherent dynamics in the charge and spin transport through a single defect in the junction between a FM contact and a nonmagnetic contact, when the magnetism of the FM oscillates in time such as during ferromagnetic resonance (FMR). During FMR and transport through the defect, the defect spin can become dynamically polarized and otherwise manipulated. In addition, analysis of the resulting oscillating current through the device allows the local spin character of the defects and their environment to be precisely determined without the use of a microwave cavity. We outline the characteristics of this effect with a defect ground-state that is either unoccupied or singly occupied by a spin-1/2 carrier, although similar features will occur for higher spin-state defects as well as those with different (but still spin-dependent) level structures. We consider the FM's magnetization to be driven periodically around an axis $\boldsymbol{\omega}_{FM}$ which is assumed to be parallel to the equilibrium magnetization, $\boldsymbol{P}_R || \hat{z}$, as depicted in Fig. 1 (green vectors). Due to the large exchange interaction within the FM, the ability for a carrier at the defect site to enter the FM is dependent on the relative orientation of the carrier's spin and the FM's magnetization. Fields local to the defect play a role in dynamically determining this relative orientation and it is through this relationship that defect spin environments can be studied via changes in the charge current. Here we consider the carriers to move from the nonmagnetic contact to the FM, so the FM is at positive bias relative to the nonmagnetic contact. We find that a *dynamic spin accumulation* forms on the defect in response to spin-selective nature of the transport into the FM. Additional Larmor precession of the defect spin, from external and local fields, resonant with ω_{FM}, can force the defect spin to either lie mostly antiparallel to the magnetization which leads to a drop in current or to interfere destructively with the FMR-induced precession which leads to a smaller time-averaged spin and a increase in current. Through a series of resonance measurements, the local field's effect on the defect spin can be fully determined, providing a sensitive, co-

herent method of defect identification. Similar features occur for the opposite bias with a ground-state spin-$1/2$ defect that has a second, unoccupied state with spin antiparallel to the ground state.

Figure 1 illustrates the details of the spin-coherent effects on charge current during FMR. Carriers situated at the defect with spin parallel to the FM magnetization, $\boldsymbol{P}_R(t)$, are transported to the FM, so the defect tends to be occupied by spin *anti-parallel* (blue) to $\boldsymbol{P}_R(t)$ (green). If γ_F, the hopping rate from the defect to the FM, is much faster than the precession frequency ($\gamma_F \gg \boldsymbol{\omega}_{FM}$), then the defect spin polarization tracks exactly anti-parallel to the rotating magnetization: $\boldsymbol{s}(t) = -\boldsymbol{P}_R(t)$. For weaker coupling the two are not firmly locked together though there is still a marked correlation between them. This correlation between $\boldsymbol{s}(t)$ and $\boldsymbol{P}_R(t)$ is a *dynamic spin accumulation* on the defect. Although there is no direct exchange coupling between the defect spin and FM, the spin filtering transport leads to an effective antiferromagnetic exchange between the two. The addition of a field (red) provides another source of precession of the defect spin: Larmor precession. When the two frequencies match and the Larmor precession is parallel to the FMR precession the defect spin locks in phase with the oscillating magnetization so any parallel spin is efficiently filtered out leaving behind a large net anti-parallel spin. The carrier spin on the defect site precesses to remain anti-parallel to the magnetization, and is thus efficiently blocked from entering the FM. As a result the charge current drops dramatically, revealing the spin-coherent properties of the defect as a resonance in the charge current itself. When the two frequencies match but the Larmor precession is perpendicular to the FMR precession, the destructive interference is at a maximum so the current displays in increase. The existence and frequencies of such resonances in the charge current identifies the defect's local field.

We now calculate the charge current through the junction under the conditions of FMR and considering the spin-coherent properties of the defect. As shown in Fig. 1 an applied bias pushes charge from the left NM to the right FM via the intermediary defect. In general the FM magnetization, $\boldsymbol{P}_R$, precesses around an axis whose orientation is indicated by spherical coordinates (α, β) at a rate ω_{FM} (shown in Fig. 1 by green precessing arrows). The external applied magnetic field is smaller than the hard axis coercive field, so the $\boldsymbol{\omega}_{FM}$ axis points parallel to the equilibrium magnetization, which is designated to be parallel to $\hat{z}$. Simultaneously the spin of the occupied defect (blue arrow) precesses in the external applied magnetic field and any local fields, $\boldsymbol{\omega}_0 + \boldsymbol{\omega}_\ell$. The ease of transport of the carrier into the FM is contingent on whether it would be a majority or minority carrier; in the case of an ideal half metal, only spins parallel to $\boldsymbol{P}_R$ would be permitted to move across the junction. For a ferromagnetic contact that is a thin film it is common for the easy axis of the contact to lie in the plane of the film; the component of the external applied magnetic field along the hard axis, if sufficiently small, does not influence the FM's precession frequency. Thus to independently control the precession frequency of the FM and the defect it suffices to control the angle of the applied magnetic field. For the analysis here we assume the applied magnetic field is mostly oriented along the hard axis of the FM, and is much smaller than the coercive field along the hard axis. Furthermore only the magnetic field component along the hard axis is varied in order to vary the defect spin's Larmor precession. As a result the precession frequency $\boldsymbol{\omega}_{FM}$ and the behavior of $\boldsymbol{P}_R$ is independent of the change in the applied magnetic field. Generalization to other regimes and geometries is straightforward.

We describe the FM magnetization as the operator $\hat{\mathbf{M}}_R(t) = \frac{1}{2}(I + \mathbf{P}_R(t) \cdot \boldsymbol{\sigma})$ which constitutes an imperfect spin filter ($\hat{\mathbf{M}}_R(t)$ is not idempotent unless $P_R = 1$) [14]. $\boldsymbol{P}_R$ precesses around $\boldsymbol{\omega}_{FM}$ and is determined by

$$\dot{\hat{\mathbf{M}}}_R(t) = -\frac{1}{2}\frac{i}{\hbar}[\boldsymbol{\omega}_{FM} \cdot \boldsymbol{\sigma}, \hat{\mathbf{M}}_R(t)]. \tag{1}$$

An analytic (if cumbersome) solution for $\hat{\mathbf{M}}_R(t)$ is readily available using an algebraic solver [15]. The density matrix of the defect spin, $\rho(t)$, also evolves in time and is determined by solving the stochastic Liouville equation which is described later in this Letter. We seek a description of the current which can encompass not only the flow of charge but also the flow of coherent spin. The 2×2 matrix $\hat{i}$ achieves this goal. The diagonal elements of $\hat{i}$ represent the movement of charge with either up or down spins and the off-diagonal elements dictate the flow of charge with up and down spin superpositions. Charge (spin) currents are then defined as $i = \mathrm{Tr}\hat{i}$ ($\boldsymbol{i}_s = \mathrm{Tr}\hat{i}\boldsymbol{\sigma}$).

This current operator is explicitly constructed by connecting the current from the NM to the defect, and from the defect to the FM, with a coherent density matrix treatment of the defect spin dynamics. The probability for a charge to pass from the defect to the FM is expressed as $\frac{1}{2}(1 + \boldsymbol{P}_d(t) \cdot \boldsymbol{P}_R(t))$. The generalization of this probability for our current operator is $\hat{\mathbf{M}}_R(t)\rho(t)$, which yields the following expression for the 'right' current (defect to FM)

$$\hat{i}_R(t) = \frac{e}{2}\gamma_R\left[\hat{\mathbf{M}}_R(t)\rho(t) + \rho(t)\hat{\mathbf{M}}_R(t)\right], \tag{2}$$

where the second term ensures hermiticity. The 'left' current (NM to defect) can be derived in a similar fashion after constraining the defect to be at most singly occupied. For greater generality the electrode can have a static magnetization,

$$\hat{i}_L(t) = e\gamma_L[1 - \mathrm{Tr}\rho(t)]\hat{\mathbf{M}}_L, \tag{3}$$

where $\hat{\mathbf{M}}_L = \frac{1}{2}(I + \mathbf{P}_L \cdot \boldsymbol{\sigma})$ is the magnetization operator of the left electrode and γ_R (γ_L) are the spin hopping rates to (from) the right (left) electrode. This formalism can be generalized to a dynamic magnetization of the left electrode, although we consider here only nonmagnetic cases where $\mathbf{P}_L = 0$.

Charge conservation demands that the 'left' current be the same as the 'right' current for a time-independent $\boldsymbol{P}_R(t)$ or when the current is averaged over an oscillation period of time-dependent $\boldsymbol{P}_R(t)$, so $\overline{\mathrm{Tr}\hat{i}_L} = \overline{\mathrm{Tr}\hat{i}_R}$. However spin conservation is not similarly required, so it is possible that $\overline{\mathrm{Tr}\hat{i}_L\sigma_z} \neq$

$\overline{\mathrm{Tr}\hat{i}_R\sigma_z}$. Construction of the defect density matrix consistently connects the charge currents and determines their sensitivity to spin and applied magnetic fields. The defect is subject to several processes (*e.g.* charge hopping on and off, applied and local fields, charge and spin blocking), and a proper theory of the defect will include its coherent evolution during these processes.

The stochastic Liouville equation is suited particularly well for this type of problem [16, 17], so we write

$$\dot{\rho}(t) = -\frac{i}{\hbar}[\mathscr{H}, \rho(t)] - \gamma_R\{\hat{\mathbf{M}}_R(t), \rho(t)\} + 2\gamma_L[1 - \mathrm{Tr}\rho(t)]\hat{\mathbf{M}}_L. \tag{4}$$

The first term of Eq. (4) represents the coherent evolution of the defect spin, the second term (curly braces are anti-commutators) denotes the spin-selective nature of tunneling into the FM. The last term describes hopping onto the defect site from the left contact. $\mathscr{H}$, the spin Hamiltonian at the defect site, is

$$\mathscr{H} = \frac{1}{2}\boldsymbol{\omega}_0 \cdot \boldsymbol{\sigma} + \frac{1}{2}\boldsymbol{\omega}_\ell \cdot \boldsymbol{\sigma} = \frac{1}{2}\boldsymbol{\omega} \cdot \boldsymbol{\sigma}. \tag{5}$$

The spin Hamiltonian consists of precession in the applied field (precession vector $\boldsymbol{\omega}_0$) and in a local field (precession vector $\boldsymbol{\omega}_\ell$), such as originates from hyperfine interactions with neighboring nuclei. In typical insulators the localization length of the defect's wave function is wide enough to encompass a large number of randomly oriented nuclei, so the local hyperfine field can be accurately approximated as a classical vector.

The defect spin density matrix is determined by numerically solving Eq. (4) and then finding the currents from either Eqs. (2) or (3). Figure 2(a) shows examples of the current evolution in a field, $\boldsymbol{\omega}$, while the magnetization precesses at $\boldsymbol{\omega}_{FM}$. It is evident that more than one oscillation mode exists; Figure 2(b) plots the power spectrum. Off-resonant oscillations (red and blue) occur at either the FMR frequency (ω_{FM}) or the defect spin's Larmor frequency (ω). On-resonant oscillations occur primarily at a single frequency ($\omega = \omega_{FM}$) but a higher order mode may also exist (not shown) for larger cone angles which is indicative of a nonlinear effect.

Under a static magnetization parallel to $\hat{z}$, current is analytically found to be [5, 7]

$$i = \frac{(1 - P_R^2\chi(\boldsymbol{\omega}))\gamma_L\gamma_R}{(1 - P_R^2\chi(\boldsymbol{\omega}))\gamma_R + 2\gamma_L}, \tag{6}$$

with

$$\chi(\boldsymbol{\omega}) = \frac{\gamma_R^2 + \omega\cos^2\theta}{\gamma_R^2 + \omega^2}. \tag{7}$$

Theoretically, by orienting the applied field along one of the cartesian axes, the local field in that direction can be determined. However as a practical matter, the linewidths are so large that distinguishing between a single and multiple defects is not viable. We now describe how to avoid this problem and uniquely identify multiple defects through these resonances.

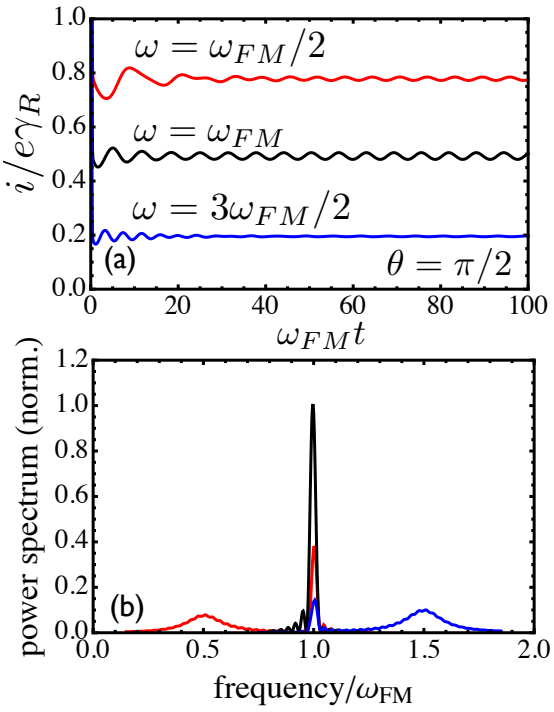

FIG. 2. (a) Charge current from three choices of the total field at the defect, ω, oriented along the x-axis. Red and blue traces are shifted ± 0.4, respectively, for clarity. Parameters are $\phi = \alpha = \beta = \beta_0 = 0$, $\alpha_0 = 0.05$ ($\sim 10\%$ cone angle), $\gamma_L = 10$, $\gamma_R = 0.1$, $P_R = 1$, $P_L = 0$. (b) Power spectrum, normalized with respect to the central peak, of the current oscillations shown in (a). The off-resonance spectra (red and blue) show shorter lived oscillations at the Larmor frequency, ω, in addition to the ferromagnetic mode.

Sweeps of the defect spin's Larmor precession frequency from the external field, ω_0, can pinpoint the local field magnitude at the defect site. First we describe how the total (external plus local) field (pointed along (θ, ϕ)) magnitude can be determined. Figure 3 shows ω scanned through the value ω_{FM} (taken as a constant). A distinct resonance appears when $\omega_{FM} = \omega$. In this way, the defect-ferromagnet system performs as a field sensor, which in principle could detect very small fields.

In real cases the defect spin precesses in at least two fields: an external field (pointing along (θ, ϕ)) and a local field. Figure 4 now separates the external field ($\omega_0 = 2\Delta\omega_\ell$ where $\Delta\omega_\ell$ is the characteristic size of the local field) and the local field, $\boldsymbol{\omega} = \boldsymbol{\omega}_0 + \boldsymbol{\omega}_\ell$, for three different external field orientations in the $x-y$ plane. Since the magnetic anisotropy energy is large, orienting the external field in this manner does not cause the FMR precession to deviate much from $\boldsymbol{\omega}_{FM} || \hat{z}$. Nor does the magnitude of ω_{FM} vary strongly with ω_0 in this configuration so, for simplicity, we take it to be a constant that must be $> \omega_{hf}$ for a resonance. If $\omega_{FM} \propto \omega_0$ an alternative restriction on the magnitude of ω_{FM} must be levied. Each orientation possesses a different resonance since ω is different in each case. Note that the results do not differ significantly between

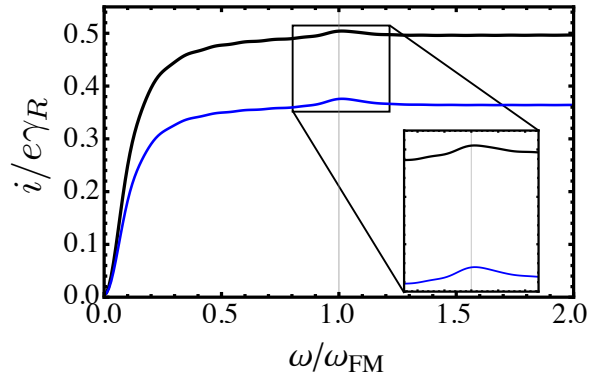

FIG. 3. (a) Current when the total field (oriented at $\theta = \pi/2$ [black] and $\theta = \pi/3$ [blue]) is swept through the value of ω_{FM}. A noticeable feature appears at $\omega = \omega_{FM}$. The resonances are magnified in the inset. The current is evaluated at $t = 50/\omega_{FM}$. Values used are $\alpha_0 = 0.05$ ($\sim 10\%$ cone angle), $\phi = \alpha = \beta = \beta_0 = 0$, $\gamma_L = 10$, $\gamma_R = 0.1$ in units of ω_{FM}, $P_R = 1$, $P_L = 0$.

the FMR (solid lines) and non-FMR (dashed lines) traces except near the resonance. The three 'measurements' of Figure 4 yield three different resonance conditions which can be used to ascertain the magnitude of each local field component via

$$\omega_{FM}^2 = \omega^2 = (\boldsymbol{\omega}_0 + (\omega_{\ell,x}, \omega_{\ell,y}, \omega_{\ell,z})) \cdot (\boldsymbol{\omega}_0 + (\omega_{\ell,x}, \omega_{\ell,y}, \omega_{\ell,z})). \tag{8}$$

The sign of $\omega_{\ell,z}$ is ambiguous, but a fourth measurement with the applied field out of the $x-y$ plane can resolve the sign. To do so may force ω_{FM} to change linearly with ω_0 in which case the resonance conditions would change. Given the positions of the resonances and external field which would be obtainable through experiments, the local field is uniquely identified to be $\boldsymbol{\omega}_\ell = (-0.582, 0.0022, 0.591)\Delta\omega_\ell$, which was the input field for this example.

Lastly this theory applies also to two independent defects through which parallel currents run. Figure 5 displays two field orientations for this scenario. Each local field is chosen randomly from a gaussian distribution of width $\Delta\omega_\ell$ and each field can be resolved by the same protocol that was used for the single defect. If a known magnetic field gradient is applied across a junction that contains two defects (whose hyperfine fields are either negligible or are already known from the previous method), then these two defects exhibit resonant phenomena as just described. However for a known field gradient, the location of the resonances can be used to extract the distance between the two defects.

Spin-coherent evolution of a defect spin produces resonant features in the charge conductivity of a ferromagnet/insulator/nonmagnet junction. From this, small numbers of defects, or a single defect, can be identified by matches between the ferromagnetic resonance frequency of a contact and the local fields of the defect(s). Demonstrating the presence of defects and their role in spin extraction, as well as identifying their origin, is vitally important to understanding spin accumulation measurements [5, 7]. The approaches described

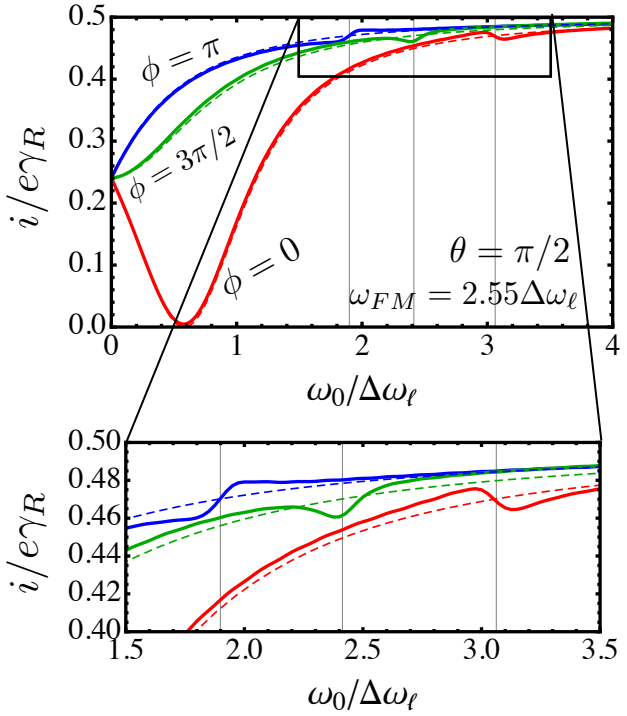

FIG. 4. (a) Resonance plots (solid lines) for three external field orientations (labeled by ϕ). Dashed lines depict current under non-FMR conditions. The local field was taken from a gaussian distribution of width $\Delta\omega_\ell$: $\boldsymbol{\omega}_\ell = (-0.582, 0.0022, 0.591)\Delta\omega_\ell$. Parameters are $\alpha = \beta = \beta_0 = 0$, $\alpha_0 = 0.05$ ($\sim 10\%$ cone angle), $\gamma_L = 10$, $\gamma_R = 0.1$, $P_R = 1$, $P_L = 0$. The current is evaluated at $\Delta\omega_\ell t = 50$. Gray vertical gridline denote resonant field determined by solving Eq. (8).

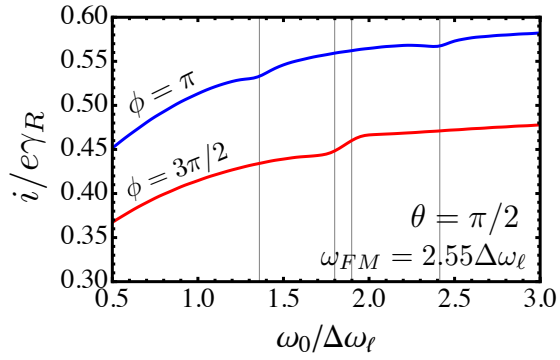

FIG. 5. Double resonance features present when two defects are probed. The two curves are displaced by 0.1 for clarity. Parameters are $\alpha = \beta = \beta_0 = 0$, $\alpha_0 = 0.05$ ($\sim 10\%$ cone angle), $\gamma_L = 10$, $\gamma_R = 0.1$, $P_R = 1$, $P_L = 0$. The current is evaluated at $\Delta\omega_\ell t = 50$. The two local fields are uniquely identified as the selected input values $\boldsymbol{\omega}_{\ell,1} = (-0.582, 0.0022, 0.591)\Delta\omega_\ell$, $\boldsymbol{\omega}_{\ell,2} = (-0.376, -1.01, 0.868)\Delta\omega_\ell$.

here would also permit the preparation of specific desired defect spin states through appropriate choices for the ferromagnet's oscillation frequency, leading to controlled studies of the coupled dynamics of two coherent spins.

Acknowledgements. — This work was supported in part by

the U.S. Department of Energy, Office of Science, Office of Basic Energy Sciences.

* nicholas-harmon@uiowa.edu
† michael_flatte@mailaps.org

[1] C. S. Wolfe, V. P. Bhallamudi, H. L. Wang, C. H. Du, S. Manuilov, R. M. Teeling-Smith, A. J. Berger, R. Adur, F. Y. Yang, and P. C. Hammel, "Off-resonant manipulation of spins in diamond via precessing magnetization of a proximal ferromagnet," Phys. Rev. B **89**, 180406 (2014).

[2] Y. Pu, P. M. Odenthal, R. Adur, J. Beardsley, A. G. Swartz, D. V. Pelekhov, M. E. Flatté, R. K. Kawakami, J. Pelz, P. C. Hammel, and E. Johnston-Halperin, "Ferromagnetic resonance spin pumping and electrical spin injection in silicon-based metal-oxide-semiconductor heterostructures," Phys. Rev. Lett. **115**, 246602 (2015).

[3] Z. Yue, D. A. Pesin, and M. E. Raikh, "Spin pumping from a ferromagnet into a hopping insulator: Role of resonant absorption of magnons," Phys. Rev. B **92**, 045405 (2015).

[4] K. Uchida, J. Xiao, H. Adachi, J. Ohe, S. Takahashi, J. Ieda, T. Ota, Y. Kajiwara, H. Umezawa, H. Kawai, G. E. W. Bauer, S. Maekawa, and E. Saitoh, "Spin seebeck insulator," Nat. Mater. **9**, 894–897 (2010).

[5] Y. Song and H. Dery, "Magnetic-field-modulated resonant tunneling in ferromagnetic-insulator-nonmagnetic junctions," Phys. Rev. Lett. **113**, 047205 (2014).

[6] O. Txoperena, Y. Song, L. Qing, M. Gobbi, L. E. Hueso, H. Dery, and F. Casanova, "Impurity-assisted tunneling magnetoresistance under a weak magnetic field," Phys. Rev. Lett. **113**, 146601 (2014).

[7] H. Inoue, A. G. Swartz, N. J. Harmon, T. Tachikawa, Y. Hikita, M. E. Flatté, and H. Y. Hwang, "Origin of the magnetoresistance in oxide tunnel junctions deter- mined through electric polarization control of the interface," Phys. Rev. X **5**, 041023 (2015).

[8] S. Baumann, W. Paul, T. Choi, C. P. Lutz, A. Ardavan, and A. J. Heinrich, "Electron paramagnetic resonance of individual atoms on a surface," Science **350**, 417–420 (2015).

[9] Jarryd J. Pla, Kuan Y. Tan, Juan P. Dehollain, Wee H. Lim, John J. L. Morton, David N. Jamieson, Andrew S. Dzurak, and Andrea Morello, "A single-atom electron spin qubit in silicon," Nature **489**, 541–545 (2012).

[10] D. D. Awschalom, L. C. Bassett, A. S. Dzurak, E. L. Hu, and J. R. Petta, "Quantum Spintronics: Engineering and Manipulating Atom-Like Spins in Semiconductors," **339**, 1174–1179 (2013).

[11] Corey J. Cochrane and Patrick M. Lenahan, "Spin counting in electrically detected magnetic resonance via low-field defect state mixing," Appl. Phys. Lett. **104** (2014).

[12] J. M. Elzerman, R. Hanson, L. H. Willems van Beveren, B. Witkamp, L. M. K. Vandersypen, and L. P. Kouwenhoven, "Single-shot read-out of an individual electron spin in a quantum dot," Nature **430**, 431 (2004).

[13] D. R. McCamey, H. Huebl, M. S. Brandt, W. D. Hutchison, J. C. McCallum, R. G. Clark, and A. R. Hamilton, "Electrically detected magnetic resonance in ion-implanted Si:P nanostructures," Appl. Phys. Lett. **89**, 182115 (2006).

[14] P. S. Farago, "Electron spin polarization," Reports Prog. Phys. **34**, 1055 (1971).

[15] The explicit forms of the matrix $\hat{\mathbf{M}}_R(t)$ for $\beta = \beta_0 = 0$ and $\alpha = 0$, which is the case we consider here, is found in the Supplementary Information.

[16] R. Kubo, J. Math. Phys. **4**, 174 (1963).

[17] R. Haberkorn, Mol. Phys. **32**, 1491 (1976).